# Association Between 18F-Fluoro-2-Deoxy-D-Glucose Uptake Values and Tumor Vitality: Prognostic Value of Positron Emission Tomography in Early-Stage Non-small Cell Lung Cancer

*Christophe Dooms, MD, PhD,* Angela van Baardwijk, MD,† Eric Verbeken, MD, PhD,‡ Robert Jan van Suylen, MD,§ Sigrid Stroobants, MD, PhD,‖ Dirk De Ruysscher, MD, PhD,† and Johan Vansteenkiste, MD, PhD**

**Introduction:** The prognostic value of quantitative 18F-fluoro-2-deoxy-D-glucose (FDG) uptake on positron emission tomography (PET) is controversial in unselected patients with non-small cell lung cancer (NSCLC). We assessed the in vivo FDG uptake, measured as maximum pixel standardized uptake value ($SUV_{max}$), in stages I and II NSCLC for its prognostic value and association with in vitro quantitative morphology of tumor vitality.

**Methods:** Prospective FDG-PET data were available in 91 consecutive patients operated for pathologic stages I and II NSCLC. Quantitative morphology was performed of tumor architecture, tumor cell density and immunohistochemical biomarkers for apoptosis (caspase-3), cell proliferation (Ki-67), hypoxia (HIF-1$\alpha$), cellular pH regulation (carbonic anhydrase IX [CAIX]), and microvessel density (CD31).

**Results:** $SUV_{max} \geq$ median and $SUV_{max}$ partial volume corrected for lesion size (PVC $SUV_{max}$) $\geq$ median were associated with an increased risk of death in univariable analysis. After correcting for stage, tumor size and age in multivariable analysis, only PVC $SUV_{max} \geq$ median remained significant. The strong significant association between tumor size and $SUV_{max}$ weakened after PVC, suggesting that an important amount of $SUV_{max}$ can be simply explained by tumor size, which is less in case for PVC $SUV_{max}$ that associates more to the tumor cell density. In multivariable logistic regression analysis, a PVC $SUV_{max} \geq$ median could be explained by high Ki-67 and high-CAIX length density.

**Conclusion:** PVC $SUV_{max}$ has a prognostic value in completely resected stages I and II NSCLC. A high-quantitative FDG uptake is associated with characteristics of tumor vitality such as high tumor cell density, high cell proliferation, and extracellular acidosis.

**Key Words:** FDG-PET scan, Non-small cell lung cancer, Prognosis, SUV.

(*J Thorac Oncol.* 2009;4: 822–828)

In 1930, Warburg[1] considered the shift in energy production from oxidative phosphorylation to glycolysis as a fundamental characteristic of a cancer cell. Dedicated positron emission tomography (PET) using 18F-fluoro-2-deoxy-D-glucose (FDG), a functional imaging technique taking advantage of this glycolytic shift, became an innovative noninvasive clinical cancer imaging for the diagnosis and the staging of non-small cell lung cancer (NSCLC). FDG is a glucose analog, which shows enhanced cellular uptake as a result of the elevated expression of the glucose transporter proteins (GLUTs) in most cancer cells. Once in the cancer cell, FDG is phosphorylated to FDG-6-$PO_4$ that cannot be further metabolized in the glycolytic pathway, thereby rendering cancer cells detectable using PET.

NSCLC is a group of carcinomas with variable biologic aggressiveness and prognosis. Clinicopathologic tumor, node, metastasis (TNM)-stage is still the most powerful prognostic factor, but even the most favorable stages, i.e., pathologic stages I and II have a 30 to 40% and 45 to 60% risk of death within 5 years after resection, respectively. Therefore, better prognostic factors are warranted. During the last decade, several retrospective analyses and one literature-based meta-analysis found that metabolic imaging relying on maximum pixel standardized uptake value ($SUV_{max}$) of the primary tumor on FDG-PET was a significant and independent prognostic factor in patients with NSCLC.[2–6] But recently, these findings also became controversial when a large prospective[7] and retrospective[8] study concluded that the prognostic role of FDG-PET seemed to be of

*Department of Pulmonology and Leuven Lung Cancer Group, University Hospitals Leuven, Belgium; †Department of Radiation Oncology (MAASTRO), GROW, University Hospital Maastricht, Maastricht, The Netherlands; ‡Department of Pathology, University Hospitals Leuven, Belgium; §Department of Pathology, University Hospital Maastricht, Maastricht, The Netherlands; and ‖Department of Nuclear Medicine, University Hospitals Leuven, Belgium.

Disclosure: The authors declare no conflicts of interest.

Christophe Dooms and Angela van Baardwijk contributed equally to this manuscript.

Address for correspondence: Christophe Dooms, MD, PhD, Department of Pulmonology (Respiratory Oncology Unit), University Hospitals Leuven, Herestraat 49, B-3000 Leuven, Belgium. E-mail: christophe.dooms@uz.kuleuven.ac.be



ISSN: 1556-0864/09/0407-0822

limited value in patients with NSCLC populations. Moreover, no clear cutoff point was found as many factors may cause methodological variability in SUV measurements across different centers (such as patient preparation procedures, scan acquisition, image reconstruction, and data analysis settings), and the relationship between the cancer cell physiology and quantitative FDG uptake on PET is less understood. Many different biologic processes may affect FDG uptake by NSCLC on both the cellular and tissue level. On the cellular level, glucose uptake is mediated by the expression of GLUT[9–11] and hexokinase-II activity,[11] and glucose demand is enhanced by cellular proliferation (which is related to Ki-67 or proliferating cell nuclear antigen expression),[9,12,13] alterations of tumor suppressor genes[14] and the expression of hypoxia-inducible-factor 1$\alpha$ (HIF-1$\alpha$).[15] On the tissue level, glucose delivery is a function of tumor perfusion that is associated with angiogenesis, anatomically reflected by microvessel density.[16] Moreover, the rate of glucose metabolism may be influenced by the presence of necrosis, reflecting that proliferation outnumbers metabolic supply, or the presence of lymphocytes and macrophages that may be confounding active metabolic cells. Additionally, tumor cells (TC) and the tumor-associated stroma (with its inflammatory interstitium, fibrocollagenous interstitium, and vasculature) should be seen as a functional domain with a metabolic cooperation between cancer cells and newly formed fibroblasts and vessels.[17]

As the evidence for the prognostic value of FDG uptake remains limited when all stages of NSCLC are considered, we conducted this translational analysis within surgically treated stages I and II NSCLC to explore the mechanisms why quantitative FDG uptake on PET may stratify patients for prognosis. We aimed to explore the potential of FDG uptake as a prognostic factor for outcome and a predictive factor for phenotyping tumor vitality. Unlike most other studies, we performed quantitative morphology of tumor architecture and quantitative immunostaining for cell proliferation (Ki-67 expression), tumor hypoxia (nuclear HIF-1$\alpha$ expression), tumor pH regulation (membranous carbonic anhydrase IX [CAIX]), cellular apoptosis (caspase-3 expression), and neoangiogenesis (CD31 microvessel density) in this study. Other factors possibly influencing FDG uptake such as tumor cell density and tumor size were also investigated.

## PATIENTS AND METHODS

### Patients

The surgical specimens of 91 consecutive patients with NSCLC (78 males, 13 females) undergoing baseline state of the art preoperative staging including FDG-PET scan and subsequently a thoracotomy with complete resection and systematic mediastinal lymph node dissection for pathologic stages I or II at University Hospitals Leuven ($n = 56$) and Maastricht ($n = 35$). The UICC classification (TNM, 6th edition, 2002) was used for pathologic staging. Only patients with pure NSCLC histology (adenocarcinoma, squamous cell carcinoma, and large cell carcinoma) were included. No adjuvant chemotherapy was given. Overall survival follow-up was obtained by patient records or by phone contact with the referring physicians.

### Dedicated FDG-PET Scan

FDG-PET scans in Leuven were performed on a CTI-Siemens (Iselin, NJ) 931/08/12 PET scanner, having an axial field of view of 10.1 cm and spatial resolution of 8 mm. The patient was positioned with the primary tumor in the filed of view of the rectilinear PET camera. Then, a transmission scan was performed before (cold transmission) to FDG injection (6.5 MBq/kg, max. 555 MBq). After FDG injection, the patient remained positioned into the PET camera, and a 60-minute dynamic study of the thorax was started, followed by a 10-minute static acquisition over the primary tumor. The standardized uptake values (SUV) of the primary tumor was calculated 60 minutes postinjection. Patients from Maastricht were scanned with an ECAT EXACT 922 CTI-Siemens (Knoxville, TN) PET scanner in Aachen, having an axial field of view of 16.2 cm and spatial resolution of 6 mm. A transmission scan was also performed before FDG injection (3.5 MBq/kg) and after a median time of 60 minutes after injection 2-D whole body emission images were acquired.

For the determination of the SUV, a volumetric Region of Interest was drawn around the primary tumor on the transaxial images. The SUV was then automatically calculated as activity concentration of FDG uptake divided by the injected dose/body weight, and the pixel with the maximum SUV was considered the $SUV_{max}$. Partial volume effects, caused by the limited sampling (at the level of a pixel size) and resolution of the PET scanner, result in underestimation of the regional FDG uptake, predominantly in tumors smaller than twice the resolution of the PET scanner. For appropriate partial volume correction (PVC), the necessary recovery coefficients were determined from a software phantom based on the spatial resolution and pixel size of the PET scanner used. The spatial resolution depends on the full width at half maximum (FWHM) of the PET device (for Leuven FWHM 13 mm and for Aachen FWHM of 7 mm). We took the largest diameter of the macroscopic lesion on resection to determine the tumor size. Finally, we used the PVC algorithm used by Vesselle et al.[12] to correct the $SUV_{max}$ of lesions $<40$ mm.

$$\text{PVC } SUV_{max} = \left(\frac{(SUV_{max} \text{ measured} - 0.25)}{\text{Recovery Coefficient}}\right) + 0.25 \text{ (ref. 12)}$$

Because of technical differences in methodology for PET scanning between Leuven and Maastricht, we did not combine the absolute $SUV_{max}$ values of both data sets. Instead we dichotomized the patient groups from Leuven and Maastricht based on their respective median $SUV_{max}$ value. Thereafter, we combined the group of patients with "$SUV_{max} <$ median" from Leuven and those with $SUV_{max} <$ median from Maastricht and considered this group as the "low $SUV_{max}$ group." The same was done for patients with a "$SUV_{max} \geq$ median," which were considered as the "high $SUV_{max}$ group."

### Quantitative Morphology of Tumor Architecture and Immunohistochemistry

Tumor analysis was performed on histologic sections stained with hematoxylin and eosin (H&E) from resection

 

specimens archived at the pathology department. From each tumor two to seven H&E sections and corresponding tissue blocks were available. An H&E section of 4-$\mu$m thickness, often the largest one, was chosen for quantitative analysis. According to the principles of stereology of biologic material outlined by Weibel,[18] the tumor was divided in compartments of interest related to the investigation of functional metabolic FDG-PET data: TC, fibroblastic connective tissue, necrosis, inflammatory interstitium (INF), and a "residu." The sum of all compartments represents 100% of the tumor and tumor architecture. The proportion of each compartment was obtained by a conventional morphometric method based on a point-counting technique using a Zeiss light microscope equipped with an eyepiece containing a reticulated counting frame and unbiased counting rule.[19] The tumor cell density was counted on a H&E section using a test line, which was randomly located.

From the original paraffin-embedded tissue block selected for quantitative analysis serial sections of 4-$\mu$m thickness were prepared for immunohistochemical stainings. Tumor cells were stained for caspase-3 (a protease playing an important role in the distal effector pathway for apoptosis), Ki-67 (a proliferation marker), and endogeneous surrogate markers of hypoxia (HIF-1$\alpha$) and pH regulation (CAIX), whereas vessels and microvessels were stained for with an endothelial marker CD31.

### KI-67 and Caspase-3

We used monoclonal mouse antihuman MIB-1 antibodies (Ki-67 antigen DAKO M7240, 1:100, 45 minutes) and antihuman caspase-3 (Cell Signaling, polyclonal, 1:50, 30 minutes). The surface density of the caspase-3 and Ki-67 immunostainings was assessed using an unbiased counting frame and unbiased counting rules and this surface density, corrected for the proportion of tumor cells (% TC), was transformed into a length density.

### CAIX and HIF-1$\alpha$

We used the mouse monoclonal antihuman CAIX antibody M75 (Slovak Academy of Sciences, Bratislava, 1:50, 45 minutes) and the mouse monoclonal antihuman HIF-1$\alpha$ antibody (BD Biosciences Pharmingen, 1:50, overnight). The CAIX length density was obtained by multiplying the tumor cell density by the proportion of membranous CAIX positivity. The surface density of HIF-1$\alpha$ immunostaining, corrected for the proportion of TC, was transformed into a length density.

### CD31

Blood vessels on histologic sections were stained with a CD31 monoclonal antibody (DAKO Cytomation, 1:50, 30 minutes). The surface density of the microvessels was measured and transformed into a length density for the entire tumor.

## Statistical Analysis

All of the statistical analyses were performed with a statistical software package, using GraphPad Prism version 4.00 for Windows (GraphPad Software, San Diego, CA). The Mann-Whitney *U* test for two groups was applied to assess the association between continuous variables. The $\chi^2$ or Fisher's exact test for two groups was applied to assess the association between categorical variables. Overall survival curves were calculated with the Kaplan-Meier method and compared by the log-rank test. A disease-free survival analysis could not be performed, as these data were not retractable for all patients. In case of multivariable logistic regression analysis and multivariable Cox regression survival analysis, SAS software was used. Multicollinearity was assessed using the Spearman correlation coefficient statistic. Statistical significance was defined as $p$ values $\leq 0.05$. All $p$ values were two sided.

# RESULTS

## Patient Characteristics

In total, 91 patients with pathologic stages I and II NSCLC were included in this analysis. There were 86% males and 14% females, 74% stages I and 26% stage II patients, and 57% squamous cell carcinomas, 29% adenocarcinomas and 14% large cell carcinomas. A median tumor size of 3.8 cm (range 0.9–10.5; mean 3.9 and SD 2.3) and 3.3 cm (range 1.0–9.5; mean 3.8 and SD 2.0) was obtained for tumors from Leuven and Maastricht, respectively. The overall median follow-up time was 41 months (range 1–95) and 61 months (range 29–95) in surviving patients.

## Prognostic Value of $SUV_{max}$ on FDG-PET

Univariable Kaplan-Meier survival analysis showed a significantly worse survival when the $SUV_{max}$ was $\geq$ median

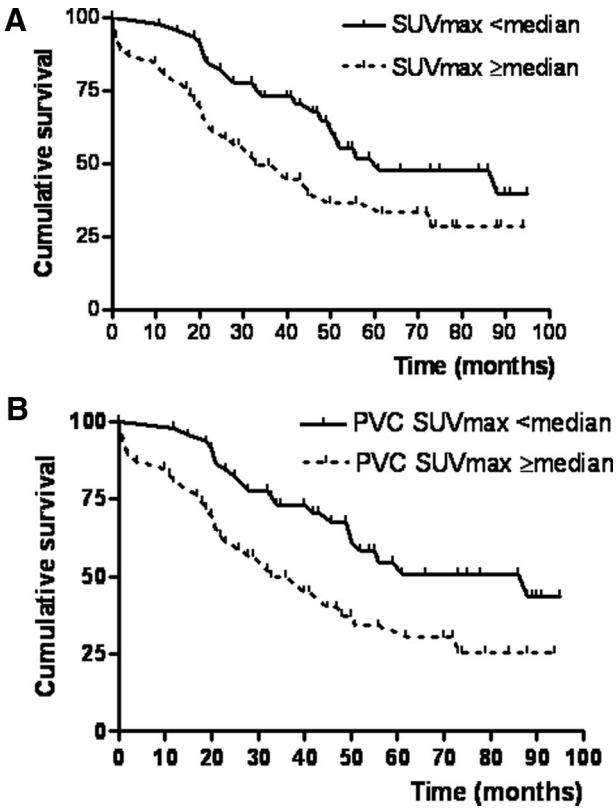


**FIGURE 1.** Kaplan-Meier overall survival curves according to median $SUV_{max}$ (*A*) and median PVC $SUV_{max}$ (*B*).

**TABLE 1.** Cox Regression Analysis of Risk of Death After Complete Resection

| | Univariable Model HR (95% CI) | Multivariable Model 1 HR (95% CI) | Multivariable Model 2 HR (95% CI) |
|---|---|---|---|
| pTNM stage | | | |
| II | 1.45 (0.78–2.93) | 1.16 (0.61–2.21) | 1.23 (0.64–2.36) |
| Age (yr) | | | |
| ≥ median | 1.74 (1.01–3.11) | 1.43 (0.78–2.62) | 1.42 (0.78–2.57) |
| T size | | | |
| ≥3 cm | 1.73 (0.97–2.96) | 1.19 (0.58–2.44) | 1.30 (0.68–2.49) |
| $SUV_{max}$ | | | |
| ≥ median | 1.87 (1.09–3.34) | 1.52 (0.79–2.94) | — |
| PVC $SUV_{max}$ | | | |
| ≥ median | 2.08 (1.21–3.73) | — | 1.88 (1.05–3.37) |

Reference categories HR 1: pTNM stage I, age < median, T size <3 cm, $SUV_{max}$ < median, PVC $SUV_{max}$ < median.
Multivariable model 1: $SUV_{max}$ adjusted for pTNM stage, age, and T size.
Multivariable model 2: PVC $SUV_{max}$ adjusted for pTNM stage, age, and T size.
HR, hazard ratio; CI, confidence interval; $SUV_{max}$, maximum pixel standardized uptake value; TNM, tumor, node, metastasis; PVC, partial volume correction.

**TABLE 2.** Association of FDG Uptake and Tumor Size, Histology, and Pathological Stage

| | $SUV_{max}$ | | | PVC $SUV_{max}$ | | |
|---|---|---|---|---|---|---|
| | < Median | ≥ Median | *p* | < Median | ≥ Median | *p* |
| T size | | | | | | |
| p-dia in cm | 2.3 (1.5–3.5) | 4.5 (3.6–5.8) | <0.0001[a] | 3.0 (2.1–4.5) | 4.1 (2.5–5.8) | 0.03[a] |
| Histology | | | | | | |
| Squamous | 25 | 27 | 0.50[b] | 24 | 28 | 0.31[b] |
| Adeno | 15 | 11 | | 16 | 10 | |
| Large cell | 5 | 8 | | 5 | 8 | |
| pTNM stage | | | | | | |
| Stage I | 37 | 30 | 0.10[c] | 34 | 33 | 0.81[c] |
| Stage II | 8 | 16 | | 11 | 13 | |
| pN stage | | | | | | |
| N0 | 41 | 38 | 0.35[c] | 39 | 40 | 1.00[c] |
| N1 | 4 | 8 | | 6 | 6 | |

[a] Mann-Whitney *U* test: median (interquartile range).
[b] $\chi^2$ test.
[c] Fisher's Exact test.
FDG, 18F-fluoro-2-deoxy-d-glucose; $SUV_{max}$, maximum pixel standardized uptake value; TNM, tumor, node, metastasis; PVC, partial volume correction.

(hazard ratio 1.87, 95% confidence interval 1.09–3.34, $p = 0.024$; Figure 1*A*) and the PVC $SUV_{max}$ was ≥ median (hazard ratio 2.08, 95% confidence interval 1.21–3.73, $p = 0.0085$; Figure 1*B*). In multivariable Cox regression analysis, only PVC $SUV_{max}$ remained significantly associated with increased risk of death after correction for pTNM stage, age, and T size (Table 1).

## Associations of FDG Uptake with Tumor Size, Histology, TNM-Stage, and N-Stage

Tumor size (as measured by the maximum diameter in the pathologic resection specimen) was significantly associated with $SUV_{max}$ ($p < 0.0001$) and PVC $SUV_{max}$ ($p = 0.03$; Table 2). Quantified FDG uptake was not significantly associated with histology, TNM stage, or N-stage but showed a trend ($p = 0.10$) for association with TNM stage that disappeared after PVC.

## Associations of FDG Uptake with Tumor Cell Density and Tumor Architecture

The tumor cell density (expressed as the number of TC per millimetre tumor) showed a significant association with $SUV_{max}$ ($p = 0.04$) and even stronger association with PVC $SUV_{max}$ ($p = 0.007$; Table 3). No association was found between FDG uptake and components of tumor architecture such as INF, necrosis, and fibroblastic connective tissue.

## Associations of FDG Uptake with Different Biologic Variables

Tables 4 and 5 summarize the univariable and multivariable analyses of the association between $SUV_{max}$ and

 

**TABLE 3.** Univariable Analysis of FDG Uptake and Quantitative Morphology on H&E Sections

| | $SUV_{max}$ | | | PVC $SUV_{max}$ | | |
|---|---|---|---|---|---|---|
| | < Median | ≥ Median | $p^a$ | < Median | ≥ Median | $p^a$ |
| *n* tumor cells/mmTC | 65 (55–80) | 75 (60–95) | 0.041 | 65 (55–75) | 80 (60–95) | 0.007 |
| % TC | 46 (28–57) | 38 (28–51) | 0.32 | 42 (28–55) | 43 (29–54) | 0.83 |
| % NEC | 3 (0–15) | 6 (3–16) | 0.12 | 6 (0–16) | 6 (1–16) | 0.64 |
| % INF | 6 (3–14) | 8 (2–16) | 0.82 | 6 (2–15) | 8 (3–15) | 0.71 |
| % FIB | 31 (21–43) | 33 (24–48) | 0.51 | 32 (23–44) | 31 (22–51) | 0.91 |

[a] Mann-Whitney *U* test: median (interquartile range).

*n*, number; TC, tumor cells; NEC, necrosis; INF, inflammatory interstitium; FIB, fibroblastic connective tissue; FDG, 18F-fluoro-2-deoxy-d-glucose; H&E, hematoxylin and eosin; $SUV_{max}$, maximum pixel standardized uptake value; PVC, partial volume correction.

**TABLE 4.** Univariable Analysis of FDG Uptake and Different Immunohistochemical Markers

| | $SUV_{max}$ | | | PVC $SUV_{max}$ | | |
|---|---|---|---|---|---|---|
| | < Median | ≥ Median | $p^a$ | < Median | ≥ Median | $p^a$ |
| *n* Ki-67/mmTC | 18 (7–27) | 22 (16–29) | 0.036 | 16 (7–24) | 23 (17–31) | 0.005 |
| *n* CAIX/mmTC | 17 (9–25) | 19 (11–31) | 0.29 | 14 (8–23) | 19 (11–33) | 0.089 |
| *N* HIF-1α/mmTC | 2 (0–9) | 4 (0–15) | 0.24 | 2 (0–9) | 5 (0–15) | 0.12 |
| *n* caspase-3/mmTC | 3 (0–8) | 5 (2–9) | 0.07 | 4 (0–9) | 5 (1–8) | 0.48 |
| *n* CD31/mm tumor | 10 (7–14) | 11 (9–14) | 0.42 | 10 (7–13) | 11 (9–15) | 0.23 |

[a] Mann-Whitney *U* test: median (interquartile range).

n, number; TC, tumor cells; HIF-1α, hypoxia; Ki-67, cell proliferation; CAIX, carbonic anhydrase IX.

**TABLE 5.** Multivariable Logistic Regression Analysis of Immunohistochemical Markers

| | Model 1: Dependent Variable: $SUV_{max}$ ≥ Median | | | | Model 2: Dependent Variable: PVC $SUV_{max}$ ≥ Median | | | |
|---|---|---|---|---|---|---|---|---|
| **Independent Variable** | **β** | ***p*** | **OR** | **95% CI** | **β** | ***p*** | **OR** | **95% CI** |
| *n* Ki-67/mm TC | 0.04 | 0.10 | 1.04 | 0.99–1.09 | 0.06 | 0.02 | 1.06 | 1.01–1.11 |
| *n* CAIX/mm TC | 0.02 | 0.24 | 1.02 | 0.99–1.06 | 0.04 | 0.05 | 1.04 | 1.00–1.07 |
| *n* HIF-1α/mm TC | 0.02 | 0.52 | 1.02 | 0.96–1.08 | 0.03 | 0.31 | 1.03 | 0.97–1.09 |
| *n* caspase-3/mm TC | 0.05 | 0.31 | 1.06 | 0.95–1.17 | −0.03 | 0.56 | 0.97 | 0.87–1.08 |
| *n* CD31/mm tumor | 0.02 | 0.73 | 1.02 | 0.93–1.10 | 0.02 | 0.63 | 1.02 | 0.94–1.12 |

Model 1, full model fitted: max $R^2 = 0.13$, Wald $\chi^2 = 8.1$, $p = 0.15$.
Model 2, full model fitted: max $R^2 = 0.20$, Wald $\chi^2 = 12$, $p = 0.036$.
HIF-1α, hypoxia; Ki-67, cell proliferation; CAIX, carbonic anhydrase IX; CI, confidence interval; TC, tumor cells.

PVC $SUV_{max}$ immunohistochemical biomarkers of different tumor functions, respectively.

Ki-67 length density was significantly associated with $SUV_{max}$ ($p = 0.036$) and even stronger with PVC $SUV_{max}$ ($p = 0.005$). CAIX and HIF-1α length density showed a trend ($p = 0.089$ and $p = 0.12$, respectively) for an association with PVC $SUV_{max}$. No association was found between quantitative FDG uptake and CD31 microvessel density.

The full model algorithm for logistic regression was applied to Ki-67, CAIX, HIF-1α, caspase-3, and CD31 length density as five independent variables and quantitative FDG uptake ≥ median as dependent variable (Table 5). The number of observations was 91, and the number of events per variable was 9.2. The fit of the full model was assessed by the Hosmer-Lemeshow goodness of fit, which was 8.5 ($p = 0.38$). After logistic regression analysis only a high Ki-67 and high-CAIX length density met the 0.05 significance level to explain a PVC $SUV_{max}$ ≥ median (Table 5).

## DISCUSSION

In this study, we assessed the prognostic value of FDG uptake in selected, i.e., pathologic stages I and II patients with NSCLC and subsequently studied the relationship of quantitative FDG uptake to various characteristics of tumor morphology and tumor vitality at a microscopic level.

The major methodological limitations of our analysis are related to the fact that older (e.g., cold transmission) PET scanners were used and that each center had its specific protocol (e.g., different FDG activities were injected, different acquisition protocols). As the scanners and acquisition protocols were standardized in each center, we assume that we may overcome these limitations by dividing the patients of each center into two groups based on the median SUV for each center.

Our study confirms in univariable analysis that the prognostic significance of quantitative FDG uptake for resected stages I and II NSCLC without adjuvant chemotherapy. As partial volume effects resulting from the limited reconstructed resolution of a PET scanner may systematically underestimate the $SUV_{max}$ in small lesions[12] and as 55% of our patients had a primary tumor <3 cm, we decided to consider both $SUV_{max}$ and PVC $SUV_{max}$ for multivariable analysis. Moreover, the prognostic value of $SUV_{max}$ can be influenced by tumor size, which is a known prognostic factor in NSCLC.[20] We observed a strong significant association between tumor size and $SUV_{max}$ ($p < 0.0001$), which clearly weakened after PVC for $SUV_{max}$ ($p = 0.03$). Nevertheless, PVC $SUV_{max}$ remained significant as a prognostic factor for overall survival in multivariable analysis for completely resected stages I and II NSCLC.

Not only the proportion of TC, but also tumor cell density was significantly associated with quantitative FDG uptake; a significant association with $SUV_{max}$ ($p = 0.04$) became stronger after PVC ($p = 0.007$). Nevertheless, one has to realize that the PVC algorithm used also may add some error as the background SUV (set at 0.25 for normal lung tissue surrounding the tumor) is not constant and as, due to the retrospective nature of this series, absence of 4D-gating precludes correction for respiratory movements. Although the presence of necrosis or inflammatory interstitium may theoretically influence quantitative FDG uptake, SUVmax, or PVC $SUV_{max}$ were not associated with these tumor compartments (Table 3).

The rationale to consider quantitative FDG uptake for assessing tumor vitality is based on the link between cancer biology and cancer biochemistry. A rapidly growing body of molecular and biochemical evidence suggests that common oncogenic signal transduction pathways underlie the mechanisms that drive both an energy dependent malignant growth signal and a fuel signal that forces the continuous cellular uptake of glucose.[21–24] Moreover, it is likely that $O_2$-regulated genes, of which HIF-1$\alpha$ is a central transcription factor, are involved in the development of a more malignant phenotype.[25] We have previously reported that the amount FDG uptake on PET is significantly associated with the expression of HIF-1$\alpha$,[15] but found now only a trend for an association (Table 4) that can be explained by the choice for a specific cut off, which is the median value in this analysis compared with a predefined 25% cut-off for HIF-1$\alpha$ previously. HIF-1$\alpha$ encodes for many proteins [24,26,27] such as glucose transporters and glycolytic enzymes that are necessary to reprogram the intracellular fate of glucose. The metabolic products of glycolysis cause intracellular acidosis that is potentially toxic for the cancer cells and might result in cellular apoptosis,[28] but HIF-1$\alpha$ also encodes for membrane bound carbonic anhydrases, such as CAIX. In multivariable regression analysis, we observed that a high-FDG uptake could be explained by high Ki-67 length density, representing cancer cell proliferation that is a requirement for disease activity, and high-CAIX length density, representing tumor pH regulation. CAIX has both an enzymatic role contributing to the maintenance of a normal intracellular pH and acidification of the extracellular environment, and a nonenzymatic role modulating cell adhesion and migration, thereby promoting a metastatic potential and poor prognosis.[29,30] In other words, a high-CAIX length density under conditions of high intracellular glucose availability can be considered an effective tumor survival strategy reflecting a metastatic phenotype and poor prognosis.

In conclusion, our study indicates that FDG-PET measuring PVC $SUV_{max}$ might have a prognostic role in completely resected pathologic stages I and II NSCLC. Whether the baseline quantitative FDG uptake could have a value in standard clinical practice for determining the indication of postoperative adjuvant chemotherapy in stages I and II NSCLC is a challenging question that deserves further study. Our translational research enabled to better characterize the relationship between PVC $SUV_{max}$ and cancer biology, finding that tumor cell density and biomarkers of cell proliferation (Ki-67 length density) and pH regulation (CAIX length density) were associated with a high-FDG uptake. To further understand the complex metabolic alterations and regulatory mechanisms during glycolysis, it is necessary that membrane receptors, key signaling pathways (PI3K-AKT, MYC and RAS-MAPK), and downstream surrogate biomarkers are prospectively analyzed together at the microscopic level.

## ACKNOWLEDGMENTS

*Supported by the Fonds voor Wetenschappelijk Onderzoek grant G.0134.04 (to C.D.) and EC FP6 funding LSHC-CT-2004-505785 (to A.V.B.).*

## REFERENCES

1. Warburg O. The Metabolism of Tumours. London: Constable Press, 1930.
2. Ahuja V, Coleman R, Herndon J, Patz E. The prognostic significance of fluorodeoxyglucose positron emission tomography imaging for patients with non-small cell lung carcinoma. *Cancer* 1998;83:918–924.
3. Vansteenkiste JF, Stroobants S, Dupont P, et al. Prognostic importance of the standardized uptake value on (18)F-fluoro-2-deoxy-glucose-positron emission tomography scan in non-small cell lung cancer: an analysis of 125 cases. *J Clin Oncol* 1999;17:3201–3206.
4. Cerfolio R, Bryant A, Ohja B, Bartolucci AA. The maximum standardized uptake values on positron emission tomography of a non-small cell lung cancer predict stage, recurrence, and survival. *J Thorac Cardiovasc Surg* 2005;130:151–159.
5. Borst GR, Belderbos JS, Boellaard R, et al. Standardised FDG uptake: a prognostic factor for inoperable non-small cell lung cancer. *Eur J Cancer* 2005;41:1533–1541.
6. Berghmans T, Dusart M, Paesmans M, et al; European Lung Cancer Working Party for the IASLC Lung Cancer Staging Project. Primary tumor standardized uptake value ($SUV_{max}$) measured on fluorodeoxyglucose positron emission tomography (FDG-PET) is of prognostic value for survival in non-small cell lung cancer (NSCLC). A systematic review and meta-analysis by the European Lung Cancer Working Party

 

for the IASLC Lung Cancer Staging Project. *J Thorac Oncol* 2008;3: 6–12.
7. Vesselle H, Freeman J, Wiens L, et al. Fluorodeoxyglucose uptake of primary non-small cell lung cancer at positron emission tomography: new contrary data on prognostic role. *Clin cancer Res* 2007;13:3255–3263.
8. Downey R, Akhurst T, Gonen M, Park B, Rusch V. Fluorine-18 fluorodeoxyglucose positron emission tomographic maximal standardized uptake value predicts survival independent of clinical but not pathologic TNM staging of resected non-small cell lung cancer. *J Thorac Cardiovasc Surg* 2007;133:1419–1427.
9. Nguyen X, Lee W, Chung J, et al. FDG uptake, glucose transporter type1, and Ki-67 expressions in non-small cell lung cancer: correlations and prognostic values. *Eur J Radiol* 2007;62:214–219.
10. Higashi K, Ueda Y, Sakurai A, et al. Correlation of GLUT-1 glucose transporter expression with 18F-FDG uptake in non-small cell lung cancer. *Eur J Nucl Med* 2000;27:1778–1785.
11. Mamede M, Higashi T, Kitaichi M, et al. [18F]FDG uptake and PCNA, Glut-1, and Hexokinase-II expressions in cancers and inflammatory lesions of the lung. *Neoplasie* 2005;7:369–379.
12. Vesselle H, Schmidt R, Pugsley J, et al. Lung cancer proliferation correlates with F18-fluorodeoxyglucose uptake by positron emission tomography. *Clin Cancer Res* 2000;6:3837–3844.
13. Higashi K, Ueda Y, Yagishita M, et al. FDG PET measurement of the proliferative potential of non-small cell lung cancer. *J Nucl Med* 2000; 41:85–92.
14. Sasaki M, Sugio K, Kuwabara Y, et al. Alterations of tumor suppressor genes (Rb, p16, p27 and p53) and an increased FDG uptake in lung cancer. *Ann Nucl Med* 2003;17:189–196.
15. van Baardwijk A, Dooms C, van Suylen RJ, et al. The maximum uptake of 18F-deoxyglucose on PET scan correlates with survival, hypoxia inducible factor-1$\alpha$ and GLUT-1 in non-small cell lung cancer. *Eur J Cancer* 2007;43:1392–1398.
16. Tateishi U, Nishihara H, Tsukamoto E, Morikawa T, Tamaki N, Miyasaka K. Lung tumors evaluated with FDG-PET and dynamic CT: the relationship between vascular density and glucose metabolism. *J Comput Assist Tomogr* 2002;26:185–190.
17. Koukourakis M, Giatromanolaki A, Harris A, Sivridis E. Comparison of metabolic pathways between cancer cells and stromal cells in colorectal carcinomas: a metabolic survival role for tumor-associated stroma. *Cancer Res* 2006;66:632–637.
18. Weibel E. Stereological Methods: Practical Methods for Biological Morphometry, Vol. 1 and 2. London: Academic Press, 1979.
19. Gundersen H, Bendtsen T, Korbo L, et al. Some new, simple and efficient stereological methods and their use in pathological research and diagnosis. *APMIS* 1988;96:379–394.
20. Mery C, Pappas A, Burt B, et al. Diameter of non-small cell lung cancer correlates with long-term survival. *Chest* 2005;128:3255–3260.
21. Blum R, Jacob-Hirsch J, Amarglio N, Rechavi G, Kloog Y. RAS inhibition in glioblastoma down-regulates hypoxia-inducible factor 1-$\alpha$, causing glycolysis shutdown and cell death. *Cancer Res* 2005;65:999–1006.
22. Elstrom R, Bauer D, Buzzai M, et al. Akt stimulates aerobic glycolysis in cancer cells. *Cancer Res* 2004;64:3892–3899.
23. Dang C, Semenza G. Oncogenic alterations of metabolism. *Trends Biochem Sci* 1999;24:68–72.
24. Lum JJ, Bui T, Gruber M, et al. The transcription factor HIF-1$\alpha$ plays a critical role in the growth factor-dependent regulation of both aerobic and anaerobic glycolysis. *Genes Dev* 2007;21:1037–1049.
25. Vaupel P, Mayer A. Hypoxia in cancer: significance and impact on clinical outcome. *Cancer Metastasis Rev* 2007;26:225–239.
26. Semenza G, Jiang B, Leung S, et al. Hypoxia response elements in the aldolase A, enolase 1, and lactate dehydrogenase A gene promoters contain essential binding sites for hypoxia-inducible factor 1. *J Biol Chem* 1996;271:32529–32537.
27. Wykoff C, Beasley N, Watson P, et al. Hypoxia-inducible expression of tumor-associated carbonic anhydrases. *Cancer Res* 2000;60:7075–7083.
28. Park H, Lyons J, Ohtsubo T, Song CW. Acidic environment causes apoptosis by increasing caspase activity. *Br J Cancer* 1999;80:1892–1897.
29. Dorai T, Sawczuk I, Pastorek J, Wiernik PH, Dutcher JP. The role of carbonic anhydrase IX overexpression in kidney cancer. *Eur J Cancer* 2005;41:2935–2947.
30. Schlappack O, Zimmerman A, Hill L. Glucose starvation and acidosis: effect on experimental metastatic potential, DNA content and MTX resistance of murine tumour cells. *Br J Cancer* 1991;64:663–670.